

Movement based inference of teleoperator state for multi-robot search

Arunim Bhattacharya¹, Abdullah Thahab¹, and Sachit Butail^{1*}

¹Department of Mechanical Engineering, Northern Illinois University, Dekalb, Illinois, USA. Contact: sbutail@niu.edu

November 27, 2024

Abstract

Human behavior encodes important information about how we perceive the environment. Extracting such information indirectly from behavioral observations has the potential to advance natural human-robot interaction without the need for wireless transmission of sensitive data. This is especially relevant in search and rescue (SAR) missions that have critical use for unmanned aerial vehicles (UAVs), which can cover large areas in a fraction of the time compared to ground-based search. In such missions, while human teleoperators typically have a range of prior knowledge about the environment or the missing person that is difficult to quantify they also experience varying workload, and may not be situationally aware at all times. An effective human-robot team would operate so that the robots would be able to adapt their search behavior in response to human state—knowledge, workload, and situational awareness—based on nonverbal movement cues of the teleoperated UAV. Accordingly, in this paper we test the hypotheses that teleoperator knowledge and state can be estimated from movement cues and that such cues can then be used to adaptively steer autonomous robots toward improved search performance. We conduct human-subject experiments in a replica of a section of the Grand Canyon National Park, which reports one of the largest number of missing person cases every year. Participants were briefed with prior knowledge about the local terrain and the missing person before every trial. EEG and eye tracking data was collected to measure cognitive load and situational awareness through multiple measures. Our results show that both search performance and turn rate of teleoperated vehicle depended on missing person knowledge. We find that cognitive load and situational awareness as measured through physiological measures are weakly correlated with movement behavior. To use these results for adaptive search, we estimate prior knowledge and situational awareness from movement data and use it in a human-swarm robot interaction strategy where multiple UAVs adapt their separation and proximity to the human teleoperator based on prior knowledge inference. Our simulation results show that adaptive search performs nearly as well as a spiral based search in terms of success rate and is able to do so in less time. Results from this work set the stage for non-verbal interaction strategies to a human-swarm setting.

1 Introduction

Between 1992 and 2007, there have been over 65,000 search and rescue (SAR) incidents in the National Parks in United States [1]. In 2005 alone there were over 2,400 SAR operations with five national parks—Grand Canyon National Park, Gateway National Recreation Area, and Yosemite National Park, Lake Mead National Recreation Area, and Rocky Mountain National Park—accounting for close to fifty percent of such incidents with the Grand Canyon National park in Arizona reporting the most such operations. Without an effective response, one in five such incidents would result in a fatality [1].

In a wilderness search and rescue (WiSAR) operation, one of the first steps is to establish a point last seen (PLS) or last known point (LKP), depending on where the missing person was last sighted or assumed present. Once a PLS is established, search areas are drawn by analyzing lost person behavior and terrain. The search areas are then prioritized based on metrics such as probability of area (POA), which is the probability that the lost person is contained within a particular region [2]. Actual search

often involves rescuers who remotely teleoperate aerial vehicles to systematically search within the POAs. Because the search area grows geometrically with time, locating a lost person alive is a time critical task.

Conventional WiSAR operations involve teams of searchers along with rescue animals on the ground coordinating with central operations to comb a large area spanning ?? square kilometers [3]. During such operations, searchers and rescuers often use small aircraft and helicopters equipped with thermal cameras to sweep inaccessible locations from air [3]. Indeed, over the past decade, unmanned aerial vehicles (UAV) are being increasingly used in WiSAR missions to find missing persons [4, 5, 6]. While completely autonomous solutions that enable terrain following [7], and swarm based solutions that cover large areas [8] are part of ongoing research, a common use of UAVs in WiSAR involves human teleoperation with a live camera feed [9, 10].

A WiSAR mission with teleoperated UAVs involves skilled operators who are expected to search efficiently within a region that has a high probability of finding the missing person. In doing so, the operators are presumed to take into account missing person behavior and terrain features [11, 12]. In reality, however, while teleoperators may be skilled in flying a UAV, they may not be familiar with the terrain they are flying over [13], or fully understand the behavior profile of the missing person in terms of how fast they may be going, their mental state, or whether they will stay near the trails [14]. While this information is available to them through other members of the WiSAR team, retaining and recovering this knowledge while flying the UAV can impose cognitive burden. Thus, prior knowledge, not skill, can be an important factor in search performance. Indeed, as has been shown in missing person models, such prior knowledge about the missing person and the terrain can significantly affect mission performance by improving the accuracy of search regions [15, 16].

In this context, inferring prior knowledge from UAV movement in the field can inform rapidly responsive control strategies. For example, in a human-swarm interaction (HSI) setup where the operator interacts directly with the swarm on the field by teleoperating a single UAV which may be considered a “leader” [17, 18], such inference can be used to control other autonomous robots in the field, who may then utilize adaptive control strategies to selectively search near or far from teleoperators [19, 20].

Because teleoperators during search have to assimilate a large amount of information in a very little time, they are also bound to experience varying degrees of cognitive burden [21, 22]. Relatedly, situational awareness (SA) is a key factor that can influence operator performance [23, 24] and is typically measured by querying operators on relevant knowledge or through physiological measures such as EEG or eye-tracking [25]. Inferring cognitive load and situational awareness directly from the movement of the UAV that is controlled by the teleoperator, therefore, has the benefit of fine-tuning the control response of autonomous UAVs nearby without having to wirelessly transmit sensitive EEG and eye tracking data.

Accordingly, this work is motivated by the following hypotheses. For a teleoperator searching for a missing person, the movement of the teleoperated UAV is affected by: (H1) prior knowledge of terrain or missing person, (H2) cognitive load of a teleoperator, and (H3) situational awareness of the teleoperator. To test these hypotheses, we conduct an experimental study where participants instrumented with an EEG and eye-tracking headset search for a missing person in a virtual 10×10 km replica of a section of the Grand Canyon National Park, which reports one of the largest number of missing person cases every year. To artificially create prior knowledge, we selectively reveal aspects of the environment and the missing person to participants before they begin the search. To additionally investigate if the presence of other UAVs affect search behavior we place UAVs that are either clustered in a random location or spread uniformly through the environment. Teleoperator movement is quantified in terms of speed, turn rate, and time spent still in place (freezing). Our results show that while prior knowledge affects speed and turn rate, cognitive load as measured using EEG and eye-tracking data is only weakly correlated to speed, turn rate, and freezing; situational awareness measured using dwell time and α power are only weakly correlated to the movement behaviors.

The experimental results are next used to evaluate an HSI search strategy where autonomous robots respond to prior knowledge inference of the human teleoperator in real time. In particular, a long short-term memory (LSTM) based classification algorithm is designed to directly infer prior knowledge from movement data of the teleoperated UAV. This classifier is then integrated into a new HSI control strategy that regulates assistance to the human based on their inferred prior knowledge. This strategy is compared to other approaches where multiple robots search independently along a

random path, follow the human teleoperator, or search in a spiral pattern.

This paper is organized as follows: section 2 reviews related work on studies that investigate teleoperator assistance strategies in SAR through intelligent interface design, dynamically changing POAs based on input from ground operations, and shared autonomy approaches where teleoperator input is blended with autonomous actions. Section 3 describes relevant background information on prior knowledge, cognitive load, and situational awareness (SA), including how cognitive load and SA can be determined using EEG and pupillometry data. Section 4 states the WiSAR problem with HSI context. Section 5 presents the experimental study including methods and results related to hypotheses H1, H2, and H3. This is followed by section 6 which describes how the LSTM model is selected to infer prior knowledge. Section 7.1 describes the multi-robot control strategy used to assist the human teleoperator in search based on prior knowledge inference. The control strategy is evaluated by comparing the performance of a human-multi-robot team where multiple robots are simulated along with the experimental human search trajectories to search for the missing target. Results of this approach is compared with other strategies in terms of fraction of trials where the human-robot team finds the target sooner than a single human and the time taken to find the missing target. We discuss the experimental and simulation results in section 8 followed by a conclusion in section 9.

2 Related work

Teleoperating a single UAV with possible assistance from autonomous UAVs is a common mode for search and rescue operations. While purely autonomous solutions are increasingly proposed in the literature, the level of risk associated with missing person search makes human involvement for detection and rescue inevitable. A WiSAR mission that utilizes teleoperated UAVs is expected to involve skilled tele-operators who may not be familiar with the local terrain [26]. Furthermore, information about the missing person themselves may be interpreted and integrated differently into search strategies by each teleoperator [13]. Interviews with SAR responders in regions with extreme climates regarding the use of UAVs have highlighted the need to assimilate vast amounts of additional information including environmental conditions and legal restrictions in addition to dealing with local capacities [27].

In this context, assistance to the teleoperator may be provided in the form of interface design which enables improved search regions [28? , 29], reduced cognitive load [30], and greater situational awareness[31, 23, 30]. Assistance may also be provided in the form of coordinated efforts between ground and aerial searchers [11], in the form shared autonomy [32], where an intelligent UAV may selectively ignore or blend human control input with its own inference of the mission, or in the form of multiple autonomous UAVs that may intelligently search the region to minimize search time [33]. This work is motivated by the last example where autonomous UAVs may assist a human teleoperator by inferring and acting on their prior knowledge.

Accessing human knowledge and skill towards improved efficiency in search is not new. For example, critical information from UAV teleoperators can be integrated with lost person behavior simulations to take search decisions [28?]. Niedzielski et al. demonstrate the effectiveness of a coordinated search and rescue strategy where teleoperators search POAs as they are assisted by imagery analysts to identify the missing person, who is then rescued by ground searchers [11]. The POAs on the map are drawn based on a lost-person mobility model that takes into account the terrain features to delineate areas of easy access by the missing person. More recently, a long-short-term memory (LSTM) networks has been used to predict human actions that are integrated into a game theoretic model to act as a decision aid to plan search and compute lost person trajectories [29], and transfer learning has been used predict human rescuers' navigation and triage strategies in urban search and rescue (USAR) missions [34].

Shared autonomy approaches include blended autonomy, where a mediation agent blends command from the tele-operator with the autonomous actions of robots based on sensory input [32], adaptive autonomy [33] where the autonomous robots decide themselves which tasks to execute, adjustable autonomy [?], where the tele-operator assigns tasks to the robots, and mixed initiative [33], where the robots and tele-operator switch between tasks depending on the level of success. Assistance from a single robot based on intent recognition was studied in [35] where a UAV acts on first-responder's movements to search within a simulated urban environment. Assistance from autonomous robots in a multi-robot setup have been explored in mutual information blending strategy [19] to provide a context independent search strategy for coordination between a teleoperator and autonomous robots.

This study focuses on enabling a similar framework through the inference of prior knowledge, cognitive load, and situational awareness from non-verbal movement cues. The use of movement cues allows communication-free and privacy-preserving implementation of robotic swarm assistance in the field.

3 Background

3.1 Prior knowledge

Prior knowledge refers to relevant information about the task at hand that could be retrieved to improve task efficiency. Prior knowledge is different from skill, for example, consider a situation where a skillful UAV operator may be searching an area not known to them. Prior knowledge has been shown to require additional cognitive capacity [36].

Examples of prior knowledge about the lost person include mental state, fatigue, and physical state, and has been shown to reduce search times significantly if considered in agent-based models [37]. Prior knowledge about terrain can include elevation, vegetation, and trails, and may be used to guide search actions such as searching within a particular region or near trails [38]. While such information may be provided to a skilled UAV operator prior to a mission, it may not be effectively utilized at all times. Furthermore, in the absence of a clear mental model of the teleoperator, it is difficult to quantify whether prior knowledge is properly utilized by a teleoperator in their search [13].

3.2 Cognitive load

Cognitive load is the mental workload experienced by a human as they perform a task [39]. During a complex time intensive task such as search and rescue, cognitive load can play a critical role in modulating task performance [40]. Specifically task performance may suffer when teleoperators have to make decisions under time pressure and cognitive limits are exceeded due to excessive information load or memory recall requirements [41].

Depending on the application, cognitive load can be measured through survey responses [42], secondary task performance [43], electroencephalogram (EEG) data [44, 45, 46], and eye-tracking data [45]. In this work, to robustify the measurement of cognitive load, we adopt a multi-pronged approach whereby we measure cognitive load using EEG and eye-tracking data. Specifically for EEG, based on prior work, we utilize the data from electrodes measuring brain activity from the frontal lobe to calculate weighted difference in spectral power over a fixed duration [46, 43]. Additionally, we use eye tracking data to calculate saccades and pupil dilation which has been shown as indicators of cognitive load [47, 48, 49].

3.3 Situational awareness

Situational awareness (SA) [50] refers to the ability to perceive, comprehend, and anticipate elements in the environment that are critical for decision-making and effective action. It involves paying attention to the environment, interpreting it correctly, and predicting how events will unfold [50].

Being situationally aware can improve safety, decision-making, and performance across a wide range of activities and time-intensive missions [51]. In this study we infer the first level of situational awareness which is generally associated with visual attention [52]. We measure SA using eye tracking data in terms of fixations rate, fixation count and, dwell time [53, 54, 55].

4 Problem statement

Consider a WiSAR scenario where a team comprising a single human teleoperated robot and a swarm of autonomous robots are searching for a missing person. Due to the large search area, the human teleoperator can only see the autonomous robot positions in an overhead view available in an inset on their feed. Compared to the human teleoperator, the autonomous robots have a lower detection rate.

We assume no communication between the teleoperator and the autonomous robots other than that they are each aware of each other's position in real time. This is because information about knowledge or cognitive state may create security vulnerabilities [56] and information coming from the

autonomous robots to the teleoperator such as video streams may pose additional cognitive burden. The goal of the mission is to find a missing person as soon as possible.

5 Experimental study

The experimental study is designed to test hypotheses H1-H3 and comprises participants teleoperating a UAV through a large virtual environment to look for a missing person as their prior knowledge is varied.

5.1 Virtual Environment

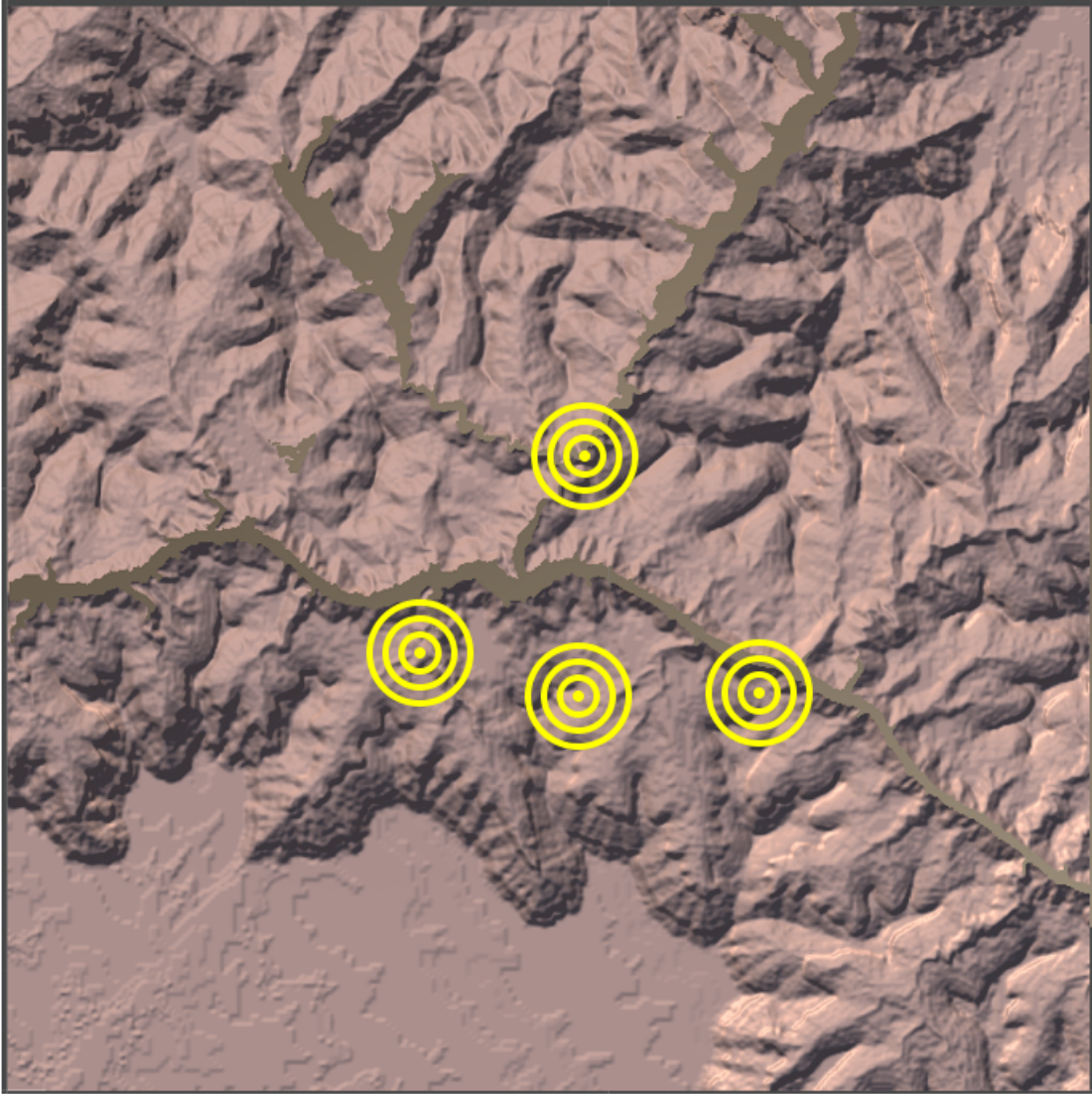


Figure 1: An overhead view of the $10 \text{ km} \times 10 \text{ km}$ virtual environment designed after the Grand Canyon National park using height map data. The four sets of concentric circles are centered at the four positions where the missing person could be last seen (PLS). One of these four locations was randomly selected for trials within the experiment. The size of the circles correspond to different distances from the PLS based on how fast the missing person may have walked since they were last sighted.

The virtual environment consisted of a $10 \text{ km} \times 10 \text{ km}$ replica of a section of the Grand Canyon

National Park (Fig.1). The park terrain was built in Unity software using height-map data obtained from an online heightmap generator [57]. The location of the terrain was approximately centered at coordinates $36^{\circ}5'57''$ N and $112^{\circ}5'38''$ W. The terrain was further enriched using trees and static water marking the Colorado River. The light brown color of the landscape was selected to match pictures of the park.

A virtual quadrotor UAV (quad-copter Simulation asset, Unity Assets) capable of flying in three dimensions was used to navigate the terrain. The operator could use arrow keys to move in front-back and left-right directions, and ‘r’ and ‘f’ keys to move up and down respectively. The UAV used realistic dynamics to simulate the motion while producing sound and rotor speeds in proportion to the thrust applied in each direction. A camera fixed to the UAV provided the teleoperator a first person view

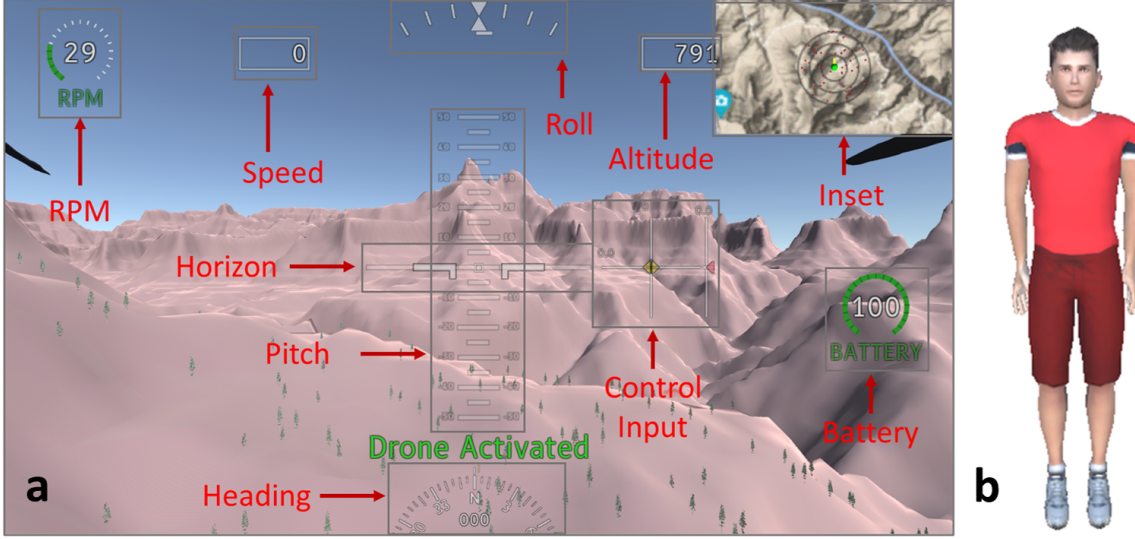


Figure 2: FPV display (a) as seen by the teleoperator. The inset in the top right corner, shows the three POAs in black circles, the position of the teleoperated UAV (filled green circle), and other UAVs (red circles). The missing person (b) was placed within random locations within the virtual environment. See video of a sample search at <https://youtu.be/3E6V3m0a7AM>

(FPV) of the environment with UAV telemetry data superimposed on the display (fig. 2). The camera could be pivoted to pitch up and down with ‘w’ and ‘s’ keys providing a front or downward facing view of the virtual environment. The FPV display (fig. 2) also showed an overhead GPS map of the environment in an inset on top right.

This inset showed the position where the missing person was last sighted (PLS), and three concentric rings marking the high probability regions called probability of areas (POAs) where the missing person may be found based on their walking speed. The radii of the POAs were set as the distance traveled by a random walker walking at speeds $s = \{1, 2, 3\}$ m/s in 36 hours. Accordingly, the average distance was calculated as $s\sqrt{\Delta t} = s\sqrt{(3600 \times 36)}$ [58], where Δt is the time for which the random walker is simulated. This translated to POAs with radii 0.36 km, 0.72 km, and 1.08 km centered at the PLS.

The missing person location was modeled after a random walker walking at a speed of 2 m/s and who stayed near the trails. Accordingly, the missing person was placed at a random location at about 0.72 km away from the PLS and within a radius of 100 m from the intersection of a trail. PLS locations were selected to be on trails that extended well beyond the largest POA radius in at least two directions. Although complex models of lost person movement that include age and mental fitness are available, we selected a simple model because the purpose of this study is to highlight the effects of prior knowledge in terms of where to search. The missing person asset was modeled as a male individual who wore a t-shirt and shorts. To further improve visibility and detectability, an emergency flare was simulated near the missing person to send out red smoke that dissipated with distance.

The position of the teleoperated UAV was shown on the inset as a green circle with a yellow line pointing in the direction of heading. To give an appearance that other robots may also be searching the environment, a swarm of 50 other UAVs were also placed randomly within in the environment and

could be seen as red circles on the inset.

5.2 Experimental Setup

The experimental setup consisted of a desktop computer with a wide-screen monitor (2560×1080 pixels, 60 Hz refresh rate, LG) to present the virtual environment, a fourteen-channel EEG device (Emotiv Epoch X, Emotiv Inc.) sampling at 256Hz to record brain activity, and an eye tracking device recording gaze position at 150 Hz (Pupil Core, Pupil Labs inc.). Lab streaming layer was used to record time-synchronized EEG, gaze, and keypress data. A chin rest was placed on the table at a fixed distance from the monitor to reduce head movement.

5.3 Experimental Conditions

The experimental conditions consisted of varying the type of prior knowledge available and the spatial distribution of the UAV swarm within the environment. Specifically, prior knowledge could be about the missing person in the form of their approximate distance from the PLS (two values, corresponding to whether such information was shown or not), terrain in the form of walking trails (two values, corresponding to whether they were shown or not), and spatial distribution of the UAV swarm (two values, spread out uniformly or clustered on a random location within the outer two POAs; the random location had no relation to the actual location of the missing person).

Correspondingly, we tested eight conditions, where each condition is encoded as a three-letter acronym depicting the presence of prior knowledge of missing person (Y/N), terrain (Y/N), and the distribution of swarm (U/C). For example, the condition NNU corresponds to where no prior knowledge was given about missing person or the terrain, and the UAV swarm were distributed uniformly through the environment; similarly the condition YYC corresponded to the prior knowledge provided for both the missing person and the terrain, and the UAV swarm clustered within the two outer POAs.

5.4 Experimental Procedure

We recruited 20 participants (16 males and 4 females, aged 24 ± 4 years) for our study. (A power analysis for repeated measures within factors. with an effect size of 0.3, power of 0.95, and a significance criterion of $\alpha = .01$ and power = .95 revealed a minimum sample size of 18.) The participants were recruited through flyers and email announcements. Candidates were excluded if they were under 18 years of age, if they wore prescription glasses to prevent potential interference with eye-tracker, or if they had thick scalp hair which could prevent EEG headset from obtaining a reliable connection with the scalp. The experiments performed here were approved by the institutional review board under protocol ID HS23-0233.

Prior to the experiment, each participant was assigned a random six-digit number and asked to review and sign a consent form. The consent form listed the purpose of the study, potential risks, and the type of data that will be collected (EEG, eye tracking, and survey responses). Participants were then asked to put on the EEG headset using a reference image. The electrodes were then adjusted until a reliable connection was obtained. This was followed by instructions on how to teleoperate the UAV, details and purpose of the search mission, meaning of the POA circles, the different information shown on the FPV display, how to indicate having found the missing person, and how to recover from a crash. This was followed by a multiple choice questionnaire given to the participants to test their understanding. Participants were next asked to put on the eye tracker which was subsequently calibrated.

The experiment began with a familiarization trial followed by eight test trials. Each participant was given a printed briefing prior to every trial including the familiarization trial. The briefing started with a paragraph describing the mission as “A person has gone missing while hiking the trails of the Grand Canyon...” and denoted that they were last seen 36 hours ago at a location marked by a circular dot on a section of the map (Fig. 3). The briefing further added that the circles centered at the PLS have radii 0.36 km, 0.72 km, and 1.08 km. Information like UAV battery time and the possibility of seeing emergency flares near the missing person was also provided within the briefing. During the familiarization trial the experimenter helped the participant find the missing person by indicating their precise location on the map on the inset. Post familiarization, the eight conditions were tested in a random order.

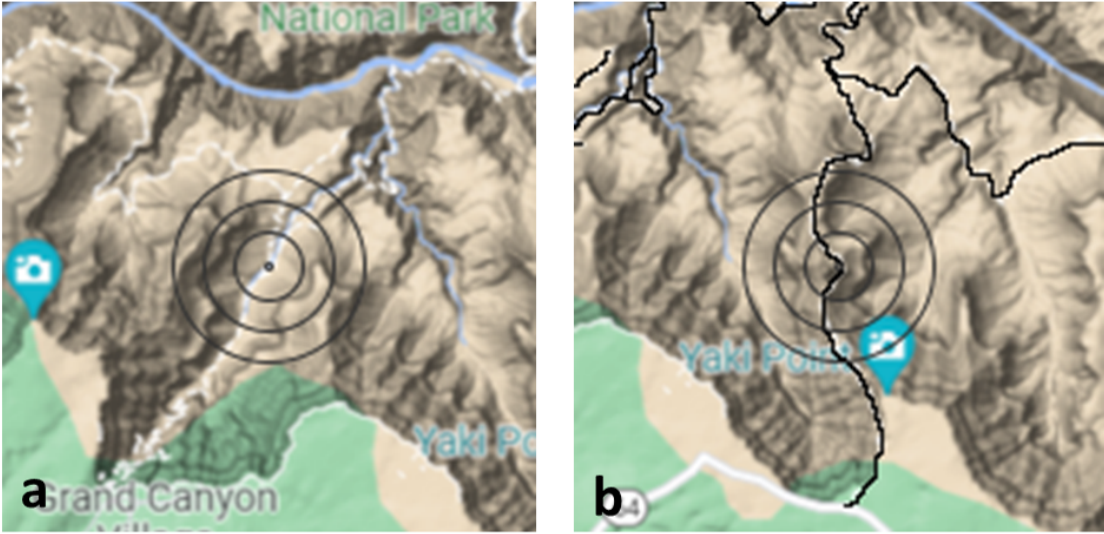


Figure 3: Overhead views shared with the participants as part of their briefings. The views obtained from Google maps were overlaid with the POAs (grey concentric circles), for conditions with no terrain knowledge (a), and with terrain knowledge (b).

During trials, additional information regarding the missing person and the terrain was provided depending on the condition being tested. Specifically, for missing person information the briefing contained italicized text that said “Based on additional information about the person physical and mental health, we think that the person may have walked between 0.36 km and 0.72 km (between smallest and the next-sized circle) during the last 36 hours”. For terrain information, the briefing contained text “Nearby trails are shown in black” on the printed map within the briefing. Figure 3 shows the two types of maps provided to participants. The search took place in one of the four locations randomly selected for a condition shown in Figure 1.

Trials ended when participants either found the missing person or at approximately 10 minutes when the battery got depleted. Upon finding the missing person, the participant was asked to enter the color of the missing person’s t-shirt and pants (one of four possible combinations) in a prompt. This was to ensure that the UAV was brought close enough for identification. At the end of every trial, the participant was asked to fill out a NASA-TLX survey to assess their mental workload in response to the trial on a 21-point scale. The participants were also offered to take a break after the fourth trial.

At the end of the experiment, participants were asked to enter their preferred gender and their age, followed by a presence questionnaire which consisted of questions on a 7-point scale. The questions surveyed the participants on their past experience with virtual reality, realism of the environment, responsiveness, where they tended to search for the missing person, and whether the presence of other UAVs affected their search.

5.5 Data analysis

Calculating movement features Trajectory data from the experiments was processed to calculate three types of movement features: speed, turn rate, and fraction of time staying still (freezing). The trajectory data was smoothed with a moving window average of 0.5 seconds and used to calculate speed and turn rate of the UAV, and time spent staying still. These features are selected as they are easily measured from the trajectory data in the field and the freezing time is expected to additionally serve as an indicator of situational awareness with a searcher possibly stopping to assess where they are in the environment and the mission [59].

Given the position $\mathbf{r}(k) \in \mathbb{R}^3$ of the UAV at k^{th} time step, the instantaneous velocity of the UAV was calculated as $\mathbf{v}(k) = \frac{\mathbf{r}(k) - \mathbf{r}(k)}{t(k) - t(k-1)}$ where $t(k)$ is the corresponding timestamp. Speed $s(k) = \|\mathbf{v}(k)\|$, is then simply the magnitude of velocity. Given the two-dimensional heading $\theta(k) \in \mathbb{R}$ of the UAV at

k^{th} time step, the instantaneous turn rate was calculated as $\omega(k) = \frac{\theta(k) - \theta(k-1)}{t(k) - t(k-1)}$. Freezing behavior was divided into two separate behaviors: freezing time when the teleoperated robot was stopped completely, quantified as the fraction of time when $s(k) \leq 0.1\text{m/s}$ and $\omega(k) \leq 0.1^\circ/\text{s}$, and turning while still which is when $s(k) \leq 0.1\text{m/s}$.

Calculating cognitive load and α -power from EEG data Cognitive load was calculated using both EEG and gaze data. With EEG data, cognitive load was calculated from the filtered data as the degree of reduction in α power denoted by frequencies within the 9.5–11.5 Hz range [46, 60]. In particular, EEG data was bandpass filtered to keep frequencies between 0.1 and 20 Hz followed by rejection of trials where any of the frontal electrodes posted an absolute amplitude above 1000 μV for greater than 5% of the length of the trial. This led to approximately 6% of the trials getting rejected. Post-filtering, for a given electrode k , the difference between the α power of baseline and trial was calculated as

$$\Delta I^k(\alpha) = I_b^k(\alpha) - I_t^k(\alpha), \quad (1)$$

where the baseline power $I_b^k(\alpha)$ is measured over data from 5 seconds prior to the start of the trial, and the trial power $I_t^k(\alpha)$ is measured over length of the trial. Cognitive load was measured as the weighted average of this difference over all the frontal electrodes as

$$L(t) = \sum_{k=1}^{14} w_k \Delta I^k(\alpha), \quad (2)$$

where the weights w_k were determined in a previous experimental study involving object identification and classification [46]. Any cognitive load value that lied beyond three times the standard deviation from the mean value across all participants was considered an outlier and removed from the dataset.

Additionally, α power has been shown to indicate level one situational awareness. We accordingly calculate over an observation window o as $I_o(\alpha) = \sum I_o^k(\alpha)$.

Calculating fixations, dwell time, saccade frequency, and pupil diameter from eye tracking data The gaze location output from the eye tracker is in terms of normalized coordinates between 0 and 1, where the extreme values correspond to the lower left corner and upper right corner of the field of view. These values were mapped to computer screen pixel coordinates with a custom application designed in windows presentation foundation software. This application which was run prior to the experiment, asked the participants to fixate at the center of a cross-hair at nine different locations on the display. A second order polynomial is then fit to the normalized coordinates (x_i, y_i) at location i to output the pixel coordinates (X_i, Y_i) as

$$\begin{aligned} X_i &= a_0 + a_1 x_i + a_2 x_i^2 + a_3 x_i y_i \\ Y_i &= b_0 + b_1 x_i + b_2 x_i^2 + b_3 x_i y_i, \end{aligned} \quad (3)$$

where, $a_{0,1,2}$ and $b_{0,1,2}$ are constants found by solving the over-determined system of equations.

A dispersion-threshold identification (I-DT) algorithm was used to quantify gaze fixation from the calibrated gaze data [61]. The I-DT algorithm identifies a group of consecutive gaze points as fixation based on an angular dispersion (how far the gaze moves during a set of consecutive points in time) and a minimum duration (how long the gaze stays within a particular region). In this study, we selected a dispersion threshold of 1° and a minimum duration threshold of 100 ms.

In our case, the dispersion threshold in degrees was converted to 8.5 mm of arc on the computer monitor using the distance of chin rest from the monitor, which was then used to determine fixation events. In particular, consecutive gaze locations were marked as fixation events if the traverse distance was less than the dispersion threshold, and cumulative time exceeded the minimum duration threshold. The output of the algorithm was individual fixation event duration and its mean location. This was used to then calculate dwell time defined as the fraction of duration of the fixation events inside an area of interest (AOI) over the duration of the full experiment. In this study, the three corners (top left, bottom left and right) with inset map size subtracted from the whole screen was considered as the AOI. The event between two fixation events is a saccadic event, the rate of such saccadic events is termed as saccadic frequency.

We use three measures of cognitive load, EEG based, pupil dilation and saccade frequency. Situational awareness is measured in terms of dwell time within the AOI and alpha power. These values are calculated over an observation window and correlated with movement features to determine which type of movement cue can be used to determine cognitive load and situational awareness of the teleoperator.

5.6 Statistical analysis

Statistical analysis to assess movement correlates of prior knowledge, cognitive load and situational awareness was performed as follows. For prior knowledge, generalized linear mixed models (GLMM) were fit to determine the dependence of speed, turn rate, and freezing time on prior knowledge. A significant effect was considered if the p value was less than 0.05. If found significant, the value of the estimate of slope compared to range was then noted to comment on the size of the effect. The main effects tested for each of the factors are swarm distribution, missing person knowledge, and terrain knowledge. For cognitive load and situational awareness, speed, turn rate, and freezing time over the length of an observation window was correlated with the cognitive load as calculated from EEG data, pupil dilation and saccade frequency for different observation windows. For situational awareness, along the same lines, speed, turn rate, and freezing time over the length of an observation window was correlated with gaze dwell time for different observation windows. In addition to these Friedman repeated measures test were performed to assess the dependence of performance on the different types of prior knowledge and spatial distribution of the swarm.

5.7 Results

Table 1: Participant response to post-experiment questionnaire.

Questions about Virtual Reality (0-6)	Response (mean \pm std)
How would you describe your past experience with VR? (rare - frequent)	1.70 \pm 1.42
How responsive did you find the virtual environment? (not responsive - very responsive)	3.40 \pm 1.19
How comfortable did you feel? (very uncomfortable - very comfortable)	3.80 \pm 1.54
How interested were you to explore the virtual environment? (not interested - very interested)	3.80 \pm 1.47
Questions about operating the UAV (0-6)	
How natural did you find the movement of the quad-rotor (UAV)? (artificial - natural)	3.30 \pm 1.63
How well could you fly through the environment? (with difficulty - with ease)	4.00 \pm 1.17
The extent to which you felt as if you were moving when standing still? (not at all - very much)	1.95 \pm 1.70
Did the presence of other UAVs affect your search? (did not - affected significantly)	1.10 \pm 1.60

Realism of the virtual environment Participants responses to questions related to the virtual environment revealed that they found the environment to be responsive and comfortable and that they were generally eager to explore the virtual environment (Table 1). In regards to operating the UAV, they found it was controllable, felt its movement to be natural, and did not experience motion sickness. Notably, participants felt that the presence of other UAVs did not affect their search.

Sample trajectories Figure 4 shows four sample data from a participant including their speed, turn rate, cognitive load, and gaze data for four out of eight trials. In general, we found that participants took about 20 seconds to start flying faster and actively searching. Participant gaze appears clustered either around the top right section of the display, which corresponded to the inset, or near the extreme right which corresponded to the battery level indicator.

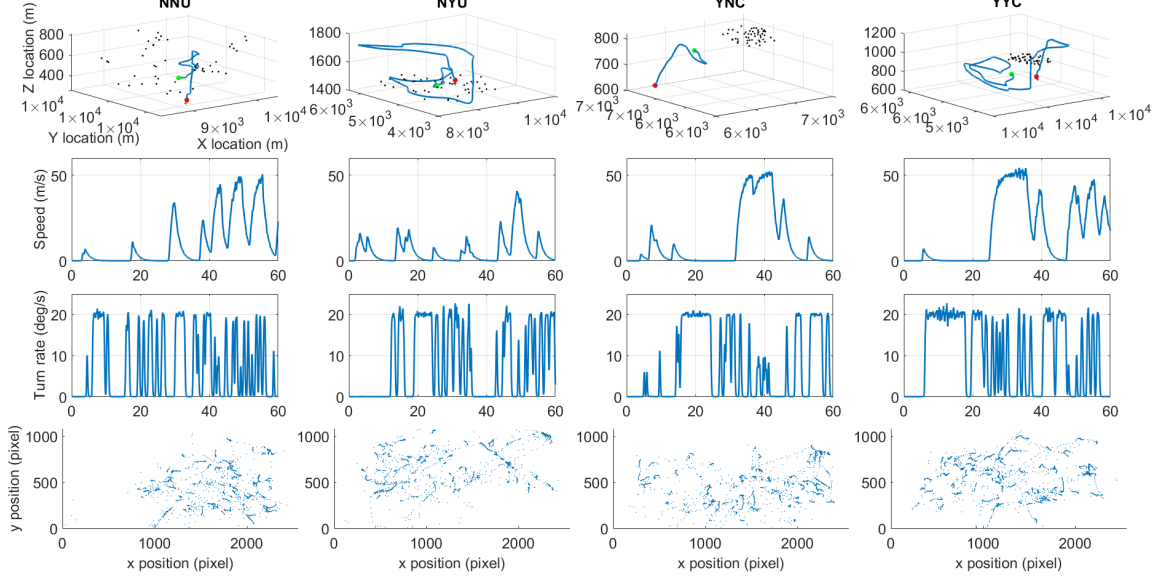


Figure 4: Sample data of a single participant showing (in rows from top to bottom) the trajectory of the teleoperated UAV, speed, turn rate, **cognitive load**, and gaze of the teleoperated UAV. Trajectory is shown for the full length of the experiment, whereas speed, turn rate, and gaze are shown for the first sixty seconds only.

Workload based on NASA-TLX survey Table 2 shows the main effects of NASA-TLX survey questions that were posed to participants after every session. The only effect that was found significant was performance, where participants perceived as having performed better when they possessed prior knowledge for missing person; although marginally significant, participants also felt less frustrated when they had prior knowledge about the missing person.

Table 2: GLMM estimates of responses to NASA-TLX questions as a function of the three independent variables.

Predictor (min, max value)	Estimate	p	Predictor (min, max value)	Estimate	p
Mental (1,21)					
Intercept	7.4	-	Intercept	10.987	-
Swarm distr (U,C)	-0.672	0.441	Swarm distr (U,C)	0.8864	0.421
Prior knowledge, missing person (N,Y)	-1.446	0.098	Prior knowledge, missing person (N,Y)	4.036	<0.001
Prior knowledge, terrain (N,Y))	-0.153	0.86	Prior knowledge, terrain (N,Y))	0.1386	0.899
Physical (1,21)					
Intercept	3.337	-	Intercept	8.787	-
Swarm distr (U,C)	0.1	0.881	Swarm distr (U,C)	-1.198	0.186
Prior knowledge, missing person (N,Y)	-0.4	0.551	Prior knowledge, missing person (N,Y)	-1.448	0.11
Prior knowledge, terrain (N,Y))	-0.475	0.478	Prior knowledge, terrain (N,Y))	-0.176	0.845
Temporal (1,21)					
Intercept	6.3	-	Intercept	5.562	-
Swarm distr (U,C)	-1.085	0.151	Swarm distr (U,C)	-0.153	0.857
Prior knowledge, missing person (N,Y)	-1.061	0.16	Prior knowledge, missing person (N,Y)	-1.627	0.056
Prior knowledge, terrain (N,Y))	-0.014	0.985	Prior knowledge, terrain (N,Y))	0.277	0.743
Frustration (1,21)					

Search performance Figure 5 shows the search performance in terms of the average time to find the target across different conditions. These values exclude participants who were not successful in finding the target (that is, who took longer than 600 seconds). Median values suggest that participants perform better when they possessed knowledge about the missing person compared to when they possessed only terrain knowledge. For example, the median performance of YNC is better than NYC, YNU is better than NYU. We also note a trend in terms of swarm distribution where a clustered swarm (that was located randomly in the environment) led to improved performance than a swarm that was distributed throughout the region.

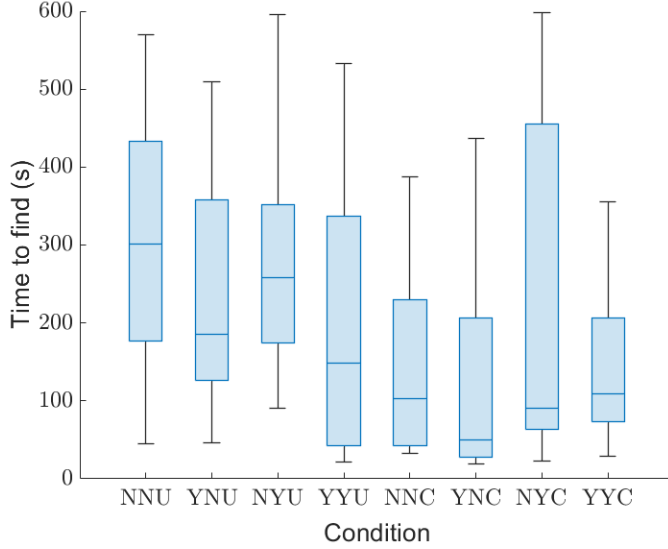


Figure 5: Post-hoc result for performance i.e. time taken to complete the mission and showing statistically significant variance between the different conditions.

Table 3: GLMM estimates of mission performance as a function of various independent factors. Values in bold indicate significant factors.

Predictor (min, max value)	Estimate	p
Performance (0,600 seconds)		
Intercept	285.468	< 0.001
Swarm distr (U,C)	-90.931	0.001
Prior knowledge, missing person (N,Y)	-66.66	< 0.016
Prior knowledge, terrain (N,Y)	2.818	0.917

Table 3 confirms these trends. We find a significant effect of swarm distribution with a clustered swarm leading to lower times to find. We also find significantly lower time to find when missing person knowledge was available. **We investigate the dependence of performance on swarm distribution further by plotting the teleoperator trajectories in the 2D plane and in terms of distance from center for the clustered and unclustered swarms (see Supplementary material).**

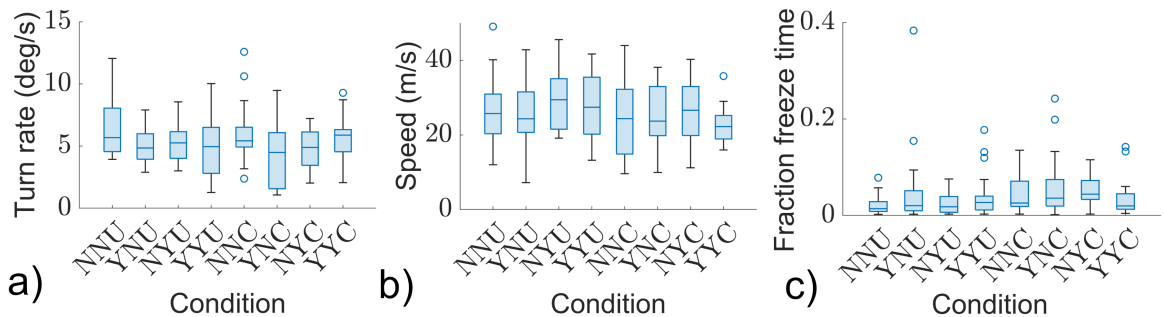


Figure 6: Plots showing a) average turn rate during trial, b) average speed during trial, c) freezing time, d) and time turning while still across experimental conditions.

Movement dependence on prior knowledge Figure 6 shows plots four different movement behaviors across experimental conditions. All values were calculated over the duration of a session. Table

Table 4: GLMM estimates of UAV movement features as a function of various independent factors. Values in bold indicate significant factors.

Predictor (min, max value)	Estimate	p
Average Speed (0, 50 m/s)		
Intercept	27.405	< 0.001
Swarm distr (U,C)	-3.152	0.0293
Prior knowledge, missing person (N,Y)	-1.488	0.303
Prior knowledge, terrain (N,Y))	1.461	0.3031
Average Turn Rate (0, 25 °/s)		
Intercept	6.165	< 0.001
Swarm distr (U,C)	-0.555	0.174
Prior knowledge, missing person (N,Y)	-0.864	0.036
Prior knowledge, terrain (N,Y)	-0.262	0.519
Freezing time (0, 1)		
Intercept	0.032	< 0.001
Swarm distr (U,C)	0.013	0.091
Prior knowledge, missing person (N,Y)	0.012	0.132
Prior knowledge, terrain (N,Y)	-0.007	0.343

4 show GLMM estimates of different movement features on independent factors in the experiment. We find that average speed of the teleoperator decreases when a swarm is clustered, and average turn rate decreases when missing person knowledge is available.

Movement correlates of cognitive load and SA Table 5 lists correlations between measures of cognitive load, situational awareness and movement features over different observation windows. Measures of cognitive load include EEG-based weighted average of difference between alpha power from test and baseline (2), pupil diameter, and saccade frequency. Measures of situational awareness include dwell time within AOI and alpha power. Movement features include turn-rate, speed, freezing time and turning while still. All these measures are calculated and correlated over 5, 10, 15 and 20 second windows.

Most cognitive load measures show no or very weak correlation with movement cues except saccade frequency which shows a weak correlation with speed at a 5 second window. Among measures of situational awareness alpha power shows a weak correlation with turning while still behavior over 15 and 20 second observation windows.

6 Estimating human prior knowledge and state based on movement cues

Based on our experimental results, which shows strong dependence of turn rate on prior knowledge and moderate dependence of turning while still behavior on situational awareness, we next build classifiers for estimating these values directly from movement cues. In particular we use LSTM to build a prior knowledge classifier and linear regression to build a situational awareness estimator.

6.1 Estimating prior knowledge

We built an LSTM network to estimate the probability of having prior knowledge about the missing person and terrain based on the movement of the teleoperator. The model was trained on over 12 hours of trajectory data collected during the experiment.

The LSTM was setup as a multi-label classifier, where the output of each type of prior knowledge was output within the range [0, 1], with 0 signifying no prior knowledge and 1 being full prior knowledge. To capture limited observation time, the trajectory data was partitioned into sections representing observation windows and the speed and turn rate data over that section served as an input to the model. The observation window size in seconds along with the mini-batch size was varied to maximize accuracy

Table 5: Correlation of cognitive load, situational awareness and movement cues

Turn rate (deg./s)				
Window size	5	10	15	20
EEG based	-0.008 (0.448)	-0.034 (0.033)	-0.039 (0.049)	-0.033 (0.149)
Pupil diameter	0.026 (0.460)	0.034 (0.510)	0.043 (0.500)	0.047 (0.530)
Saccade frequency	0.068 (0.059)	0.067 (0.188)	0.083 (0.193)	0.119 (0.125)
Dwell Time	0.0447(<0.001)	0.056(<0.001)	0.0578(0.002)	0.0733(<0.001)
Alpha power	0.0109(0.305)	0.028(0.063)	0.017(0.367)	0.012(0.594)
Speed (m/s)				
Window size	5	10	15	20
EEG based	0.038 (<0.001)	0.098 (<0.001)	0.100 (<0.001)	0.071 (0.002)
Pupil diameter	0.060 (0.095)	0.066 (0.202)	0.081 (0.206)	0.067 (0.368)
Saccade frequency	0.136 (<0.001)	0.124 (0.016)	0.119 (0.058)	0.056 (0.474)
Dwell Time	0.0158(0.145)	-8e-4(0.958)	-0.022(0.243)	-0.039(0.0793)
Alpha power	-0.017(0.107)	-0.0391(0.010)	-0.033(0.073)	-0.041(0.057)
Freezing time (fraction)				
Window size	5	10	15	20
EEG based	0.005 (0.620)	0.049 (0.001)	0.066 (<0.001)	0.082 (<0.001)
Pupil diameter	-0.008 (0.468)	-0.009 (0.537)	-0.009 (0.636)	-0.013 (0.552)
Saccade frequency	0.025 (0.024)	0.069 (<0.001)	0.052 (0.006)	0.045 (0.039)
Dwell Time	-0.055(<0.001)	-0.06(<0.001)	-0.062(0.001)	-0.043(0.049)
Alpha power	0.068(<0.001)	0.073(<0.001)	0.083(<0.001)	0.082(<0.001)
Turning while still (fraction)				
Window size	5	10	15	20
EEG based	0.016 (0.133)	0.075 (<0.001)	0.100 (<0.001)	0.116 (<0.001)
Pupil diameter	-0.007 (0.529)	-0.007 (0.659)	-0.007 (0.700)	-0.009 (0.676)
Saccade frequency	-0.008 (0.472)	0.072 (<0.001)	0.055 (0.004)	0.058 (0.008)
Dwell Time	-0.074(<0.001)	-0.0797(<0.001)	-0.074(<0.001)	-0.0546(0.013)
Alpha power	0.108(<0.001)	0.114(<0.001)	0.127(<0.001)	0.136(<0.001)

of the model defined as [??](#). Hyperparameter sets included observation window size of {5, 10, 15, 20} seconds and [mini-batch sizes of ??](#).

The initial neural network architecture selected for LSTM was based on [\[62\]](#) which has been shown to work well for time-series classification. The original model was adapted to enable two input features, and instead of multi-class classification, a multi-label classification was used. To optimize the model, we used a variation of k-fold cross validation to find the optimal hyper parameters as described in the algorithm [1](#). Figure [7](#), shows the neural network architecture used in this study. Fig. [8](#) shows average maximum accuracy as a function of observation time. We selected an observation of 15 seconds and [a mini-batch size of ??](#) that produced the maximum average accuracy of 0.7 ± 0.07 .

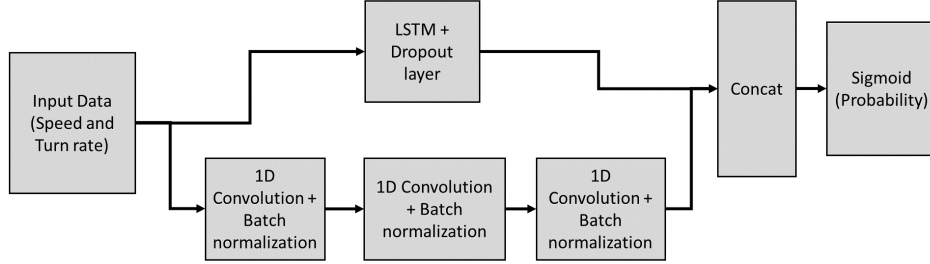


Figure 7: The neural network architecture as used in this paper.

Algorithm 1 k-Fold algorithm to obtain optimal parameter set for LSTM training.

Dataset D , K_1 outer iterations, K_2 inner iterations and, P parameter sets.

```

for i = 1 to  $K_1$  do
    randomize  $D$  dataset by subjects
     $train_1 \leftarrow$  80% of randomized dataset
     $test_1 \leftarrow$  20% of randomized dataset
    for j = 1 to  $K_2$  do
        randomize  $train_1$  dataset by subjects
         $train_2 \leftarrow$  80% of  $train_1$  dataset
         $test_2 \leftarrow$  20% of  $test_1$  dataset
        for each  $p$  in  $P$  parameter set do
             $M2 \leftarrow$  create model with  $p$  parameters
            train  $M2$  with  $train_2$  dataset
            validate  $M2$  with  $test_2$  dataset
        end for
    end for
    Select the hyper parameter set  $p$  with highest validation accuracy
     $M1 \leftarrow$  create model with selected hyper parameters
    train  $M1$  with  $train_1$  dataset
    validate  $M1$  with  $test_1$  dataset
end for
Select hyper-parameters of observation window size and mini-batch size that produce highest averaged maximum accuracy
  
```

6.2 Estimating situational awareness

We used linear regression to estimate SA from the fraction of time spent turning while still over an observation window of 15 seconds selected to match the observation time for prior knowledge estimation. Specifically, given f_{turn} as the fraction of time spent turning while still, we fit a line to the resulting alpha power to obtain the relation

$$I_{15}(\alpha) = 0.34698 + 11.228f_{turn}. \quad (4)$$

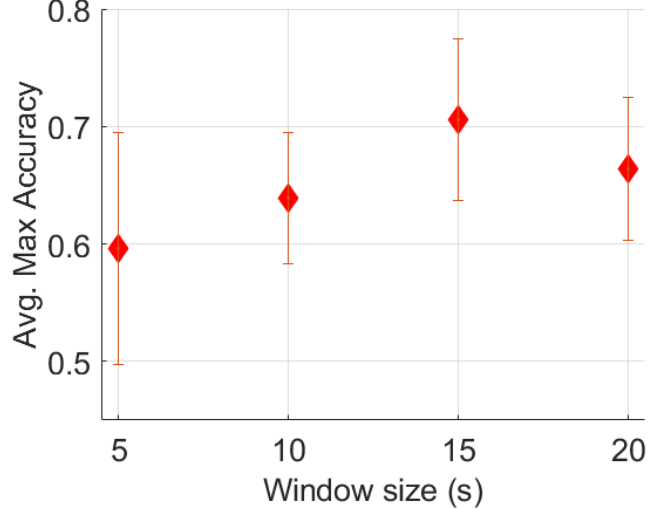


Figure 8: Average maximum accuracy plots.

The resulting alpha power is then normalized so that it lies between 0 and 1 as

$$\hat{I}_{15}(\alpha) = \frac{I_{15}(\alpha) - I_{15}(\alpha)_{min}}{I_{15}(\alpha)_{max} - I_{15}(\alpha)_{min}}. \quad (5)$$

7 Swarm response to prior knowledge inference and SA

7.1 Control strategies

In this section we formulate closed loop control strategies for an autonomous swarm that is informed by the estimated prior knowledge and situational awareness of the human operator within a human-robot team. These strategies are compared with traditional spiral search patterns and random search patterns in terms of success rate and time to find the missing person.

The autonomous robot swarm moves according to a modified version of the kinematic self-propelled particle model called the zonal model [63]. Specifically, the position $\mathbf{r}_i(t) \in \mathbb{R}^3$ and velocity $\mathbf{v}_i(t) \in \mathbb{R}^3$ of i -th autonomous robot at time t is updated to avoid collisions, align with neighbors, and remain within a certain range of the swarm, all while preferentially following the human operator. The velocity of a robot i is updated as

$$\mathbf{v}_i(t + \delta t) = \begin{cases} -s_i \mathbf{d}_{i,zor}(t) & \text{if } zor_i \neq \emptyset \\ 0.5 s_i ((\mathbf{d}_{i,zoo}(t) + \mathbf{d}_{i,zoa}(t))(1 - k_h) + k_h \mathbf{d}_{i,n}) & \text{otherwise,} \end{cases} \quad (6)$$

where,

$$\mathbf{d}_{i,zor} = \sum_{j \in zor} -\frac{\mathbf{r}_i - \mathbf{r}_j}{|\mathbf{r}_i - \mathbf{r}_j|}, \quad \mathbf{d}_{i,zoo} = \sum_{j \in zoo} \frac{\mathbf{v}_j}{|\mathbf{v}_j|}, \quad \text{and} \quad \mathbf{d}_{i,zoa} = \sum_{j \in zoa} \frac{\mathbf{r}_i - \mathbf{r}_j}{|\mathbf{r}_i - \mathbf{r}_j|},$$

and $\mathbf{d}_{i,h} = \frac{\mathbf{r}_h - \mathbf{r}_i}{|\mathbf{r}_h - \mathbf{r}_i|}$; $zoo(t)$, $zor(t)$, and $zoa(t)$ denote the time varying sets of neighbors that lie within a distance zoo , zor , and zoa ; i and j represent focal agent and neighboring agent respectively ($i \neq j$); h is the subscript for the human participant, and $\delta t = ?$ denotes the simulation time step in seconds; $s_i \in \mathbb{R}$ denotes constant speed. Model parameters zoo , zor , and zoa , can be varied to produce different types of behavior [63].

We maintain a zor value of r_{fov} to (a) ensure minimal overlap of field of view between robots towards and efficient search and (b) prevent clustering even though it led to an improved performance in our experiments to avoid inefficient feedback loops that may arise from the participant following the swarm towards false alarms.

This model is updated with a gain parameter k_h which determines how strongly a robot follows the human teleoperator. The missing person and terrain knowledge are denoted by $P_K(t)$ and, $T_K(t)$ respectively, the detection radius $r_{fov} = 100$ m) and, $k_h(t)$ gain is used to modify the behavior

Table 6: Control Loop strategies in extreme cases of prior knowledge.

P_K	T_K	Action	Justification
1	0	Large separation of swarm, strong following	Increased coverage over the same terrain
0	1	Low swarm separation and strong following	Strong overlap in the same terrain because terrain knowledge.
1	1	Large separation, very strong following	Increased coverage in the same terrain
0	0	Small separation, weak following	Not trusting the human operator, swarm searches randomly

In case of the closed loop control strategy, the action of the swarm is under absolute condition i.e. when the probabilities of the available prior knowledge is either 0 or 1 are summarized in table 6. If the human operated UAV has no knowledge about the terrain or the missing person, the swarm searches randomly and doesn't trust the human at all, if only missing person knowledge is available there would be large separation between the UAVs and the swarm would somewhat follow the human, in case where both the knowledge are available, the swarm completely trusts the human and would follow the human strongly with large separation.

- a) **Search based on person and terrain knowledge** The zor of the swarm determined by terrain knowledge so that high terrain knowledge of the teleoperator leads to smaller value of zor and tighter coverage of the region around the human teleoperator. Person knowledge directly affects the tendency of the swarm to follow the teleoperated UAV as

$$zor(t) = r_{fov}(0.9 + e^{-10.5T_k}), \quad (7)$$

$$k_h(t) = P_K(t), \quad (8)$$

- b) **Search based on person knowledge only** Person knowledge directly affects the tendency of the swarm to follow the teleoperated UAV.

$$k_h(t) = P_K(t), \quad (9)$$

- c) **Search based on person and terrain knowledge, and SA** The zor of the swarm is determined by terrain knowledge and person knowledge affects the gain k_h regulated by SA as

$$zor(t) = r_{fov}(0.9 + e^{-10.5T_k}) \quad (10)$$

$$k_h(t) = k_{SA}P_K(t), \quad (11)$$

where $k_{SA} = I(\hat{\alpha})$.

- d) **Search based on person knowledge with SA** person knowledge affects the gain k_h regulated by SA as

$$k_h(t) = k_{SA}P_K(t), \quad (12)$$

- e) **Random search** In this strategy, the UAV swarm ignores the teleoperated UAV, this is achieved by setting $k_h = 0$.

- f) **Spiral search** In this strategy, the UAV swarm follows a spiral trajectory achieved by using a modified version of 6 where the first agent of the swarm follows a predetermined spiral trajectory and the rest of the agents follow the first agent with a gain g ,

$$\mathbf{v}_{i,i \neq 1}(t + \delta t) = \begin{cases} -s_i \mathbf{d}_{i,zor}(t) & \text{if } zor_i \neq \emptyset \\ 0.5s_i ((\mathbf{d}_{i,zoo}(t) + \mathbf{d}_{i,zoa}(t))(1-g) + g\mathbf{d}_{i,1}) & \text{otherwise,} \end{cases} \quad (13)$$

where, $\mathbf{d}_{i,1} = \frac{\mathbf{r}_1 - \mathbf{r}_i}{|\mathbf{r}_1 - \mathbf{r}_i|}$; 1 is the index for the first agent in the swarm.

7.2 Simulation setup

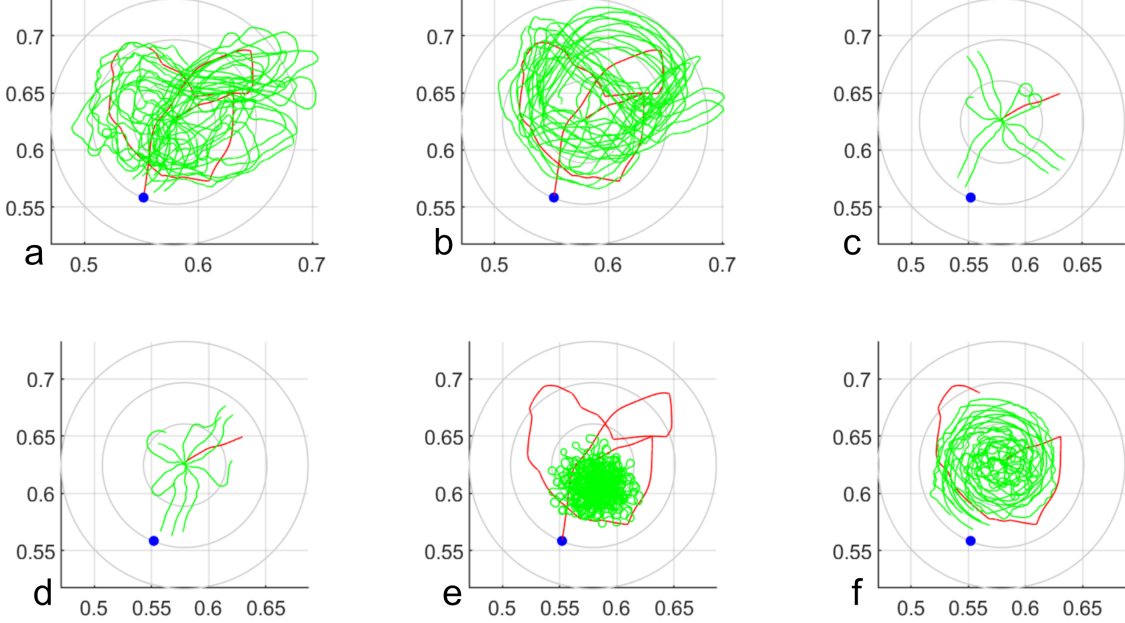


Figure 9: Trajectories of participant and autonomous swarm in the order listed in section 7.1, for the same condition. The grey circles represent the three POAs for the location, the blue dot represents location of the missing person, the red line shows trajectory of the participant and the green lines show swarm trajectory.
update after rerun and do not show participant trajectory on e and f

Figure 10: Prior knowledge and SA estimates for 4 sample trajectories of a participant. The trajectories are same as in Figure 4

In order to test the different search strategy, a simulation which plays back the trajectory of the participant is setup. In the original experiment, the swarm of autonomous robots were either clustered in a random location or spread out uniformly over the search area, however in the simulation the swarm exhibit different behaviors depending on the search strategy. The closed loop control strategy uses a neural network trained in python using tensorflow module exported for C#.

A dedicated environment was setup in unity for the simulation, the terrain is identical to the one used in the experiment. This environment plays back the participants' recorded trajectory, however it is interpolated with a time step of 0.04 s . A swarm of autonomous UAV is initialized at the location of the person last seen. Figure 9 shows the top view of the simulation environment with position last seen (PLS) represented by a black dot and probability of area (POA) shown in grey circles are projected on the map. In our case we set the value of $zor = r_{fov}$ and $zoo = zor + 8$ and $zoa = zoo + 14$ to correspond with the dynamic parallel behavior in [63].

Figure 9, shows instance of a random search strategy by a swarm of 5 robots, the human operated robot trajectory is played back as recorded during the experiment. The swarm behavior is coded differently for different search strategy, a) human operated UAV follows a spiral pattern with a width of r_{fov} with the same speed as that of the average speed of the participants in the experiment as the rest of the swarm follows the human with $k_h = 1$ and matching its speed with the teleoperator, b) human operated UAV follows a spiral pattern with the same speed as that of the average speed of the participants in the experiment as the rest of the swarm with $k_h = 0$ with the average human speed, c) swarm ignores the human operated UAV in case of random search with the average human speed, d) swarm follows the human in case of follow search matching the human speed, e) swarm operates on a control strategy as described in section 7.1 matching the human speed.

The swarm robots are positioned at approximately 170 m above the lowest elevation of the map, with a field of view of about 30°, each robot of the swarm can sense presence of the missing person within a 100 m radius directly below it. Every robot in the swarm travels at a constant speed of 50 m/s. All search strategies were tested for 5, 10 and 20 swarm size.

A false alarm behavior is coded into all search strategies, where individual UAV agents slow down to investigate an area close to a false alarm location. For a search strategy, the maximum speed is denoted by s_{max} , and its speed is given as,

$$s_i(t) = \frac{s_{max}}{1 + e^{-0.08(d_{false}^{i,j}(t)-48.6)}} + \frac{s_{max}}{1 + e^{0.08(d_{false}^{i,j}(t)+48.6)}} \quad (14)$$

Where, $s_i(t)$ is the speed of i -th agent in the swarm and $d_{false}^{i,j}(t)$ is the distance of i -th agent from j -th false alarm location, $j = 1, 2$ representing one of 2 locations of false alarms.

Each experimental condition was simulated once, thus providing 160 instances (8 conditions × 20 subjects) of search for every swarm size. The criteria for a successful swarm search is: a) the missing person was found with a probability of detection of 0.6 and, b) swarm found the missing person 15 seconds prior to the end time recorded for the condition.

7.3 Simulation results

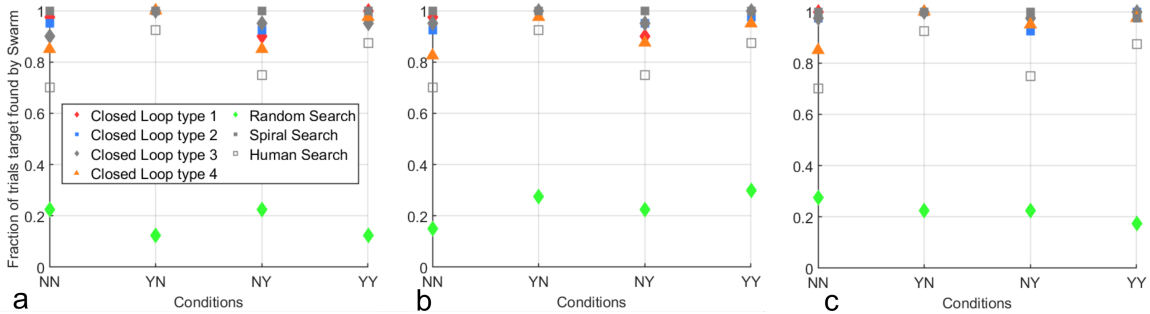


Figure 11: Simulation result showing fraction of trials that the target was found using a swarm size of 5, 10 and, 15 robots.

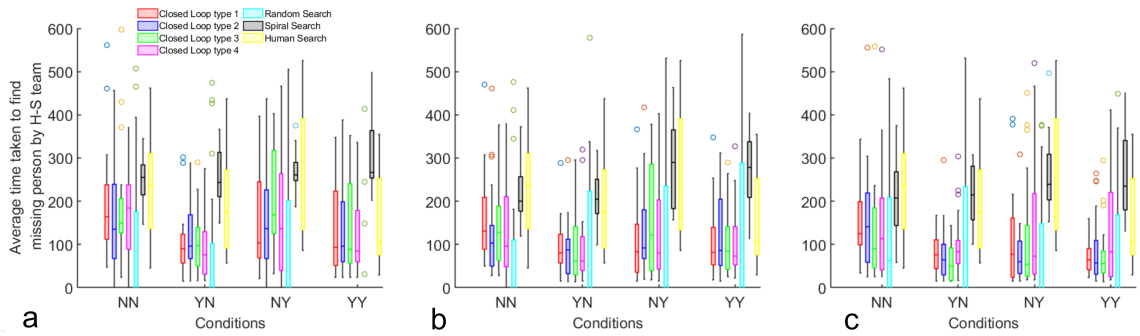


Figure 12: Simulation results showing average time gained over time taken by participants using a swarm size of 5, 10 and, 15 robots.

8 Discussion

Executing a SAR mission with a teleoperated UAV involves taking multiple time-critical decisions. In such a scenario, prior knowledge about the mission would admittedly play an important role. Quantifying this effect on performance, mental workload, and behavior has implications in shared autonomy and user interface design. Furthermore, the perception of other UAVs in the region may influence the actions and in turn performance of the teleoperator. This study was designed to isolate these effects by artificially creating prior knowledge in the form of pre-trial briefings and placing a swarm of UAVs in different spatial distributions. Our results point to several significant effects of prior knowledge and swarm perception on performance, cognitive load, perception and behavior.

In terms of workload as measured using NASA-TLX, the tasks were not perceived to be physically demanding, however the participants felt they had to put considerable effort to accomplish the tasks. Low frustration levels indicate that the experiment design was not a significant barrier to accomplishing the task, further supported by the favorable responses regarding the virtual environment and the teleoperation of the UAV.

Placement of UAV clusters were purposefully made to be randomly placed between the middle and outer POAs because in this study our principal goal is to observe the effect of prior knowledge on search performance with a secondary goal of influencing the operator behavior using UAV clusters. In the briefing for cases where the prior knowledge about a human is present, we emphasize that the missing person may be somewhere between the middle and outer POA. Mission performance was strongly influenced by the presence of swarm in a cluster and missing person knowledge. It is possible that although the UAV swarm was not necessarily located near the missing person, having it at the same approximate distance from the PLS enabled the participants to waste less time searching within the smaller POA where the missing person was never actually located. If the swarm cluster was placed in the general vicinity of the missing person, the results probably would have diluted the effects of our primary goal. One of the limitation of this study is that the UAV swarm was static, if the simulation had involved a moving swarm cluster, we would be able to observe how teleoperator behavior changes with changing behavior of the swarm further, this would have enabled us to use the clustered swarm behavior as an input to the LSTM prior knowledge inference model.

Presence of terrain knowledge did not lower the time to find, likely because there were multiple trails for each location, not available on the inset, so that participants may have lost precious time investigating these areas between the display and the printed briefing. Indeed, participants spent more time fixating on the inset when terrain knowledge was available. Missing person knowledge positively affected mission performance, probably due to the fact that during briefing we mention to the participant the probable distance traveled by the missing person and which reduces their area of search, this sentiment was echoed by the participants as well, evidenced by their responses to the performance question on NASA-TLX.

Cognitive load as measured using three metrics doesn't show strong correlation with movement behavior of the participants, this could be because the mission difficulty was not high enough to exert the mental faculties of the participants, they probably were just casually looking for the missing person. It is partially confirmed by the NASA-TLX questionnaire about mental effort. Perhaps a stronger correlation would be observed if only the high performing trials were used in the statistics.

Situational awareness (SA) was also found to be only weakly correlated with movement behavior, this could be because of the indirect way we are measuring SA. The conventional way of measuring SA by freezing the simulation to pose SAGAT questionnaire was deemed too intrusive for the mission at hand, thus we settled on indirect measures of SA.

9 Conclusion

In this study we create a virtual reality environment mimicking a section of the Grand Canyon National Park, where participants were asked to look for a missing person of a given description. The participant was provided with prior knowledge by selectively revealing information about the terrain and/or the missing person. To gauge their cognitive load and situational awareness, EEG and gaze were recorded. We found that missing person knowledge significantly affected their performance. It was theorized that missing person prior knowledge of the teleoperator can be leveraged to improve the search times if we were to involve a swarm of autonomous robots to aid the teleoperator. An LSTM model was

trained to take speed and turn rate of the operator as input and output prior knowledge levels of the operator. We found that such a system outperforms other search strategies with a sufficiently high swarm size.

A natural extension of this work will be to repeat this experiment with a swarm of robots that change their search strategies in real-time in response to the movement behavior of the participant.

10 Acknowledgments

This research was supported by National Science Foundation under grant # IIS-2033918.

References

- [1] Travis W Heggie and Michael E Amundson. Dead men walking: search and rescue in us national parks. *Wilderness & environmental medicine*, 20(3):244–249, 2009.
- [2] Paul J. Doherty, Quinghua Guo, Jared Doke, and Don Ferguson. An analysis of probability of area techniques for missing persons in yosemite national park. *Applied Geography*, 47:99–110, February 2014.
- [3] Aron Dick. *Arizona Basic Search and Rescue*. 2023.
- [4] Norbert Tuśnio and Wojciech Wróblewski. The efficiency of drones usage for safety and rescue operations in an open area: A case from poland. *Sustainability*, 14(1):327, December 2021.
- [5] Michael A. Goodrich, Bryan S. Morse, Damon Gerhardt, Joseph L. Cooper, Morgan Quigley, Julie A. Adams, and Curtis Humphrey. Supporting wilderness search and rescue using a camera-equipped mini uav. *Journal of Field Robotics*, 25(1–2):89–110, December 2007.
- [6] Grogan S, Pellerin R, and Gamache M. The use of unmanned aerial vehicles and drones in search and rescue operations—a survey. In *Proceedings of the PROLOG*, page 1–13, 2018.
- [7] Mario Silvagni, Andrea Tonoli, Enrico Zenerino, and Marcello Chiaberge. Multipurpose uav for search and rescue operations in mountain avalanche events. *Geomatics, Natural Hazards and Risk*, 8(1):18–33, Oct 2016.
- [8] S Nunnally, P Walker, A Kolling, N Chakraborty, M Lewis, K. Sycara, and M Goodrich. Human influence of robotic swarms with bandwidth and localization issues. Oct 2012.
- [9] Jeffrey Delmerico, Stefano Mintchev, Alessandro Giusti, Boris Gromov, Kamilo Melo, Tomislav Horvat, Cesar Cadena, Marco Hutter, Auke Ijspeert, Dario Floreano, Luca M. Gambardella, Roland Siegwart, and Davide Scaramuzza. The current state and future outlook of rescue robotics. *Journal of Field Robotics*, 36(7):1171–1191, Aug 2019.
- [10] Jason Isaacs, Kevin Knoedler, Andrew Herdering, Mishell Beylik, and Hugo Quintero. Teleoperation for urban search and rescue applications. *Field Robotics*, 2(1):1177–1190, Mar 2022.
- [11] Tomasz Niedzielski, Mirosława Jurecka, Bartłomiej Miziński, Joanna Remisz, Jacek Śłopka, Waldemar Spallek, Matylda Witek-Kasprzak, Łukasz Kasprzak, and Małgorzata Świerczyńska-Chłaściak. A real-time field experiment on search and rescue operations assisted by unmanned aerial vehicles. *Journal of Field Robotics*, 35(6):906–920, 2018.
- [12] Robert James Koester. *Lost person behavior : a search and rescue guide on where to look for land, air, and water*. Charlottesville, Va Dbs Productions, 2008.
- [13] Michael D. Coover Jennifer L. Burke, Robin R. Murphy and Dawn L. Riddle. Moonlight in miami: Field study of human-robot interaction in the context of an urban search and rescue disaster response training exercise. *Human–Computer Interaction*, 19(1-2):85–116, 2004.
- [14] William G Syrotuck. *Analysis of Lost Person Behavior*. 2000.

- [15] Lanny Lin and Michael A. Goodrich. A bayesian approach to modeling lost person behaviors based on terrain features in wilderness search and rescue. *Computational and Mathematical Organization Theory*, 16(3):300–323, Jul 2010.
- [16] Amanda Hashimoto, Larkin Heintzman, Robert Koester, and Nicole Abaid. An agent-based model reveals lost person behavior based on data from wilderness search and rescue. *Scientific Reports*, 12(1), Apr 2022.
- [17] Andreas Kolling, Phillip Walker, Nilanjan Chakraborty, Katia Sycara, and Michael Lewis. Human Interaction With Robot Swarms: A Survey. *IEEE Transactions on Human-Machine Systems*, 46(1):9–26, February 2016.
- [18] Andreas Kolling, Phillip Walker, Nilanjan Chakraborty, Katia Sycara, and Michael Lewis. Human interaction with robot swarms: A survey. *IEEE Transactions on Human-Machine Systems*, 46(1):9–26, 2015.
- [19] Rafal Krzysiak and Sachit Butail. Information-based control of robots in search-and-rescue missions with human prior knowledge. *IEEE Transactions on Human-Machine Systems*, 52(1):52–63, 2021.
- [20] Larkin Heintzman, Amanda Hashimoto, Nicole Abaid, and Ryan K Williams. Anticipatory planning and dynamic lost person models for human-robot search and rescue. In *2021 IEEE International Conference on Robotics and Automation (ICRA)*, pages 8252–8258. IEEE, 2021.
- [21] Brennan Jones, Anthony Tang, and Carman Neustaedter. Remote communication in wilderness search and rescue: Implications for the design of emergency distributed-collaboration tools for network-sparse environments. *Proc. ACM Hum.-Comput. Interact.*, 4(GROUP), jan 2020.
- [22] Nathan D Rasmussen, Bryan S Morse, Michael A Goodrich, and Dennis Eggett. Fused visible and infrared video for use in wilderness search and rescue. In *2009 Workshop on Applications of Computer Vision (WACV)*, pages 1–8. IEEE, 2009.
- [23] ” where am i?” acquiring situation awareness using a remote robot platform. In *2004 IEEE International Conference on Systems, Man and Cybernetics (IEEE Cat. No. 04CH37583)*, volume 3, pages 2835–2840. IEEE, 2004.
- [24] LJ Sorensen and NA Stanton. Y is best: How distributed situational awareness is mediated by organisational structure and correlated with task success. *Safety Science*, 56:72–79, 2013.
- [25] Endsley MR. A systematic review and meta-analysis of direct objective measures of situation awareness: A comparison of sagat and spam. *Human Factors: The Journal of the Human Factors and Ergonomics Society*, 63(1):124–150, 2021.
- [26] Yangming Shi, John Kang, Pengxiang Xia, Oshin Tyagi, Ranjana K. Mehta, and Jing Du. Spatial knowledge and firefighters’ wayfinding performance: A virtual reality search and rescue experiment. *Safety Science*, 139:105231, Jul 2021.
- [27] Dylan G. Clark, James D. Ford, and Taha Tabish. What role can unmanned aerial vehicles play in emergency response in the arctic: A case study from canada. *PLOS ONE*, 13(12):e0205299, Dec 2018.
- [28] I.R. Nourbakhsh, K. Sycara, M. Koes, M. Yong, M. Lewis, and S. Burion. Human-robot teaming for search and rescue. *IEEE Pervasive Computing*, 4(1):72–78, Jan 2005.
- [29] Larkin Heintzman and Ryan K Williams. A predictive autonomous decision aid for calibrating human-autonomy reliance in multi-agent task assignment. *arXiv preprint arXiv:2112.10252*, 2021.
- [30] Michael Baker, Robert Casey, Brenden Keyes, and Holly A Yanco. Improved interfaces for human-robot interaction in urban search and rescue. In *2004 IEEE International Conference on Systems, Man and Cybernetics (IEEE Cat. No. 04CH37583)*, volume 3, pages 2960–2965. IEEE, 2004.

- [31] Jennifer M. Riley and Mica R. Endsley. The hunt for situation awareness: Human-robot interaction in search and rescue. *Proceedings of the Human Factors and Ergonomics Society Annual Meeting*, 48(3):693–697, Sep 2004.
- [32] Ryan Wegner and John Anderson. Agent-based support for balancing teleoperation and autonomy in urban search and rescue. *International Journal of Robotics and Automation*, 21(2):120–128, 2006.
- [33] Benjamin Hardin and Michael A Goodrich. On using mixed-initiative control: A perspective for managing large-scale robotic teams. In *Proceedings of the 4th ACM/IEEE international conference on Human robot interaction*, pages 165–172, 2009.
- [34] Yue Guo, Rohit Jena, Dana Hughes, Michael Lewis, and Katia Sycara. Transfer learning for human navigation and triage strategies prediction in a simulated urban search and rescue task. In *2021 30th IEEE International Conference on Robot & Human Interactive Communication (RO-MAN)*, pages 784–791. IEEE, 2021.
- [35] Dimitri Ognibene, Lorenzo Mirante, and Letizia Marchegiani. Proactive intention recognition for joint human-robot search and rescue missions through monte-carlo planning in pomdp environments. In *Social Robotics: 11th International Conference, ICSR 2019, Madrid, Spain, November 26–29, 2019, Proceedings 11*, pages 332–343. Springer, 2019.
- [36] Bruce K. Britton and Abraham Tesser. Effects of prior knowledge on use of cognitive capacity in three complex cognitive tasks. *Journal of Verbal Learning and Verbal Behavior*, 21(4):421–436, August 1982.
- [37] W. Mohibullah and Simon J. Julie. Developing an agent model of a missing person in the wilderness. In *2013 IEEE International Conference on Systems, Man, and Cybernetics*. IEEE, October 2013.
- [38] Ashish Macwan, Julio Vilela, Goldie Nejat, and Beno Benhabib. A multirobot path-planning strategy for autonomous wilderness search and rescue. *IEEE transactions on cybernetics*, 45(9):1784–1797, 2014.
- [39] Fred Paas, Juhani E. Tuovinen, Huib Tabbers, and Pascal W. M. Van Gerven. Cognitive load measurement as a means to advance cognitive load theory. *Educational Psychologist*, 38(1):63–71, March 2003.
- [40] Thomas R. Colin, Nanja J.J.M. Smets, Tina Mioch, and Mark A. Neerincx. Real time modeling of the cognitive load of an urban search and rescue robot operator. In *The 23rd IEEE International Symposium on Robot and Human Interactive Communication*. IEEE, August 2014.
- [41] Bethan Moncur, Maria J. Galvez Trigo, and Letizia Mortara. *Augmented Reality to Reduce Cognitive Load in Operational Decision-Making*, page 328–346. Springer Nature Switzerland, 2023.
- [42] John Sweller, Paul Ayres, and Slava Kalyuga. *Measuring Cognitive Load*, pages 71–85. Springer New York, New York, NY, 2011.
- [43] E. W. Anderson, K. C. Potter, L. E. Matzen, J. F. Shepherd, G. A. Preston, and C. T. Silva. A user study of visualization effectiveness using eeg and cognitive load. *Computer Graphics Forum*, 30(3):791–800, June 2011.
- [44] Gregory Bales and Zhaodan Kong. Cognitive correlates of eeg spectral power indicate human-swarm task performance. In *Proceedings of the 8th International Conference on the Internet of Things, IOT ’18*. ACM, October 2018.
- [45] Bhanuka Mahanama, Yasith Jayawardana, Sundararaman Rengarajan, Gavindya Jayawardena, Leanne Chukoskie, Joseph Snider, and Sampath Jayarathna. Eye movement and pupil measures: A review. *Frontiers in Computer Science*, 3, January 2022.

- [46] Arunim Bhattacharya and Sachit Butail. Measurement and analysis of cognitive load associated with moving object classification in underwater environments. *International Journal of Human–Computer Interaction*, 40(10):2725–2735, January 2023.
- [47] Johannes Zagermann, Ulrike Pfeil, and Harald Reiterer. Studying eye movements as a basis for measuring cognitive load. In *Extended Abstracts of the 2018 CHI conference on human factors in computing systems*, pages 1–6, 2018.
- [48] Jeff Klingner, Rakshit Kumar, and Pat Hanrahan. Measuring the task-evoked pupillary response with a remote eye tracker. In *ETRA '08: Proceedings of the 2008 symposium on Eye tracking research applications*, pages 69–72, New York, NY, USA, 2008. ACM.
- [49] Krzysztof Krejtz, Andrew T Duchowski, Anna Niedzielska, Cezary Biele, and Izabela Krejtz. Eye tracking cognitive load using pupil diameter and microsaccades with fixed gaze. *PloS one*, 13(9):e0203629, 2018.
- [50] Mica R Endsley. Toward a theory of situation awareness in dynamic systems. *Human factors*, 37(1):32–64, 1995.
- [51] John D Lee. Fifty years of driving safety research. *Human factors*, 50(3):521–528, 2008.
- [52] Ting Zhang, Jing Yang, Nade Liang, Brandon J Pitts, Kwaku Prakah-Asante, Reates Curry, Bradley Duerstock, Juan P Wachs, and Denny Yu. Physiological measurements of situation awareness: a systematic review. *Human factors*, 65(5):737–758, 2023.
- [53] Lucas Paletta, Amir Dini, Cornelia Murko, Saeed Yahyanejad, Michael Schwarz, Gerald Lodron, Stefan Ladstätter, Gerhard Paar, and Rosemarie Velik. Towards real-time probabilistic evaluation of situation awareness from human gaze in human-robot interaction. In *Proceedings of the companion of the 2017 ACM/IEEE international conference on human-robot interaction*, pages 247–248, 2017.
- [54] Sogand Hasanzadeh, Behzad Esmaeli, and Michael D Dodd. Examining the relationship between construction workers’ visual attention and situation awareness under fall and tripping hazard conditions: Using mobile eye tracking. *Journal of construction engineering and management*, 144(7):04018060, 2018.
- [55] S Merchant, Yongjin Kwon, T Schnell, T Etherington, and T Vogl. Evaluation of synthetic vision information system (svis) displays based on pilot performance. In *20th DASC. 20th Digital Avionics Systems Conference (Cat. No. 01CH37219)*, volume 1, pages 2C1–1. IEEE, 2001.
- [56] Chao Lin, Debiao He, Neeraj Kumar, Kim-Kwang Raymond Choo, Alexey Vinel, and Xinyi Huang. Security and privacy for the internet of drones: Challenges and solutions. *IEEE Communications Magazine*, 56(1):64–69, 2018.
- [57] Cities-skylines-heightmap-generator. <https://github.com/sysoppl/Cities-Skylines-heightmap-generator>, 2022.
- [58] Papoulis, A. (1984b) *Probability, Random Variables and Stochastic Processes*. Singapore: McGraw Hill.
- [59] Richard T Stone, Michael Dorneich, Stephen Gilbert, and Elease McLaurin. Human differences in navigational approaches during tele-robotic search. In *Proceedings of the Human Factors and Ergonomics Society Annual Meeting*, volume 57, pages 625–629. SAGE Publications Sage CA: Los Angeles, CA, 2013.
- [60] Wolfgang Klimesch. Eeg alpha and theta oscillations reflect cognitive and memory performance: a review and analysis. *Brain research reviews*, 29(2-3):169–195, 1999.
- [61] Dario D Salvucci and Joseph H Goldberg. Identifying fixations and saccades in eye-tracking protocols. In *Proceedings of the 2000 symposium on Eye tracking research & applications*, pages 71–78, 2000.
- [62] Fazle Karim, Somshubra Majumdar, Houshang Darabi, and Shun Chen. Lstm fully convolutional networks for time series classification. *IEEE Access*, 6:1662–1669, 2018.

- [63] Iain D Couzin, Jens Krause, Richard James, Graeme D Ruxton, and Nigel R Franks. Collective memory and spatial sorting in animal groups. *Journal of Theoretical Biology*, 218(1):1–11, 2002.